Competing two-phase coexistence in doped manganites: Direct observations by *in situ* Lorentz electron microscopy

J. Q. He,[1,*,†] V. V. Volkov,[1,*,‡] T. Asaka,[1,§] S. Chaudhuri,[2,‖] R. C. Budhani,[2,3] and Y. Zhu[1]

[1]*Condensed Matter Physics and Material Science Department, Brookhaven National Laboratory, Upton, New York 11973, USA*

[2]*Condensed Matter-Low Dimensional Systems Laboratory, Department of Physics, Indian Institute of Technology Kanpur, Kanpur 208016, India*

[3]*National Physical Laboratory, New Delhi 110012, India*

We examined thin epitaxial films $La_{5/8-y}Pr_yCa_{3/8}MnO_3$ (LPCMO: $y=0.275-0.3$) *in situ* by Lorentz transmission electron microscopy (TEM) and other microscopy methods. Clear evidence was obtained for the competing two-phase coexistence of antiferromagnetic charge-ordered (CO) and ferromagnetic (FM) phases that exhibit mesoscale phase separation below the metal-to-insulator transition (MIT) at ~164 K. In addition, we observed some regions of mixed CO- and FM-domain contrast attributed earlier to formation of the new CO-FM phase. Using *in situ* heating/cooling TEM experiments, we interpret this effect as the interfacial wetting phenomenon inherent to the first-order CO-FM phase transition, rather than to the formation of new CO-FM phase. It is evidenced by the partial magnetic melting of CO phase at interfaces with the FM phase, thereby creating charge-disordered spin-glass metastates. For coexisting CO- and FM-domain configurations, we directly refined the relationship between charge-orbital and spin-ordering vectors, consistent with FM moments pinned by (101)-crystal twins in LPCMO films. We also discuss the striking linear dependence observed below MIT for the log-resistance behavior and the CO fraction in LPCMO directly measured by TEM. Such linear dependence does not follow typical percolation equations, suggesting that percolation model needs further revisions for transport description of manganites.

I. INTRODUCTION

Many doped manganese perovskite oxides, $R_{1-x}M_xMnO_3$ (R=La, Pr, Nd, and Sm and M=Ca, Sr, Ba, Pb, and Te) show mixed-phase behavior in the doping range $0.3 \leq x \leq 0.5$ in agreement with the general predictions by Goodenough[1] derived from semicovalent exchange theory, and the double-exchange mechanism for Mn^{3+}/Mn^{4+} ion balance in a perovskite-type $LaMnO_3$ lattice. Of special interest is the very strong dependence of transport properties, including the critical parameters of the metal-to-insulator transition (MIT), on the effect of the coexistence of the ferromagnetic metallic (FMM) and the antiferromagnetic (AFM) phases, also known as the charge-ordered insulating (COI) phase. Experimentally, the delicate balance between the FMM-COI phases may alter due the subtle changes in various factors, such as chemical doping, temperature, and the magnetic and electrical fields. These features of the mixed-valence manganites have attracted considerable scientific and technological interest due to their remarkable electronic and magnetic properties. Some of them are FM metals at low temperatures in zero magnetic fields, but upon heating they lose their magnetic order with a concomitant increase of several orders of magnitude in their electrical resistivity. One such a remarkable material in the manganite family is the mixed-valence compound $La_{5/8-y}Pr_yCa_{3/8}MnO_3$ (LPCMO) that shows colossal magnetoresistance (CMR) and transport properties sensitive to y doping[2–4] including other intriguing phenomena[5–9] that are not well understood due to the system's complexity. Thus, even with fixed Ca doping ($x=3/8$) optimized for the magnetic Curie (T_c) point[1,10] the y tuning of La/Pr ratio in LPCMO may switch from the FMM ground state at $y=0$ toward the dominant COI state at $y=5/8$.[9] While such features are ubiquitous for LPCMO at $0 \leq y \leq 5/8$, the topology and the energetic aspects of the electrical, magnetic, and structural states of the material below and above the MIT temperature remain enigmatic. Indeed, despite a great deal of work, we still are far from good understanding the microscopic nature of the phase-separated states in manganites. For example, the electronic properties of the constituent phases, their volume fractions, and their spatial distributions in samples remain to be characterized. More importantly, the physical mechanism underlying the phase-separation phenomenon for the FMM- and AFM-ordered domains is unclear. On the other hand, direct transmission electron microscopy (TEM) observations suggest that electronic-phase separation in manganites may be observable at two different length scales: (a) at the nanoscale (~10–20 nm) and (b) at the mesoscale (submicron). For example, nanoscale separation was observed by Becker *et al.*[11] in $La_{0.7}Sr_{0.3}MnO_3$ and $La_{0.7}Ca_{0.3}MnO_3$ with scanning tunneling microscopy, by Mori *et al.*[12] in Cr-doped $Nd_{0.5}Ca_{0.5}MnO_3$ with Lorentz TEM (LTEM) and, more recently, by Tao *et al.*.[13] in $La_{1-x}Ca_xMnO_3$ with scanning electron nanodiffraction. On the other hand, Chen and Cheong[14] observed phase separation on a submicron scale in $La_{0.5}Ca_{0.5}MnO_3$, supported by the similar observations of Uehara *et al.*[2] for $La_{1-x-y}Pr_yCa_xMnO_3$ at $y=0.375$ down to 20 K; these authors also proposed the existence of a percolation mechanism for electron transport in mixed manganites through the FMM phase embedded in the CO insulating matrix. Soon thereafter, Loudon *et al.*[15] reported the occurrence of submicron scale FM and CO domains in the compound $La_{0.5}Ca_{0.5}MnO_3$ at 90 K. In addition, they identified a small region that ap-

pears to be both an FM metal and a CO insulator, the unexpected so-called CO ferromagnetic (CO-FM) phase. Furthermore, earlier in 2002 Mori *et al.*[16] had noted the presence of both states in small areas of an $La_{5/8-y}Pr_yCa_{3/8}MnO_3$ ($y=0.375$) sample. These observations were surprising because, expectedly, the FMM and COI in manganites are mutually exclusive ground states. A growing number of experiments on electron transport[6,9] and diffraction studies[17,18] suggest that the simple percolation model in manganites needs further revision, possibly by including another charge-disordered (CD) phase while the traditional CO phase should play a less important role[17] in the overall MIT mechanism. Accordingly, more experimental work is required on the microstructure of manganites to resolve these basic questions, including the origin of the CMR effect.

In our current experimental work with LTEM-TEM methods, we examined both the microstructure and magnetic behavior of single-crystal films $La_{5/8-y}Pr_yCa_{3/8}MnO_3$ (LPCMO: $y=0.275-0.3$) at the low-temperature limit and at the mid-temperature interval close to the magnetic transition at $T_c \sim 170$ K. We explored the modes of stabilization and conversion of the CO and FM states at different temperatures that play an important role in the phase transition from insulator to metal. We focus on the strong magnetic anisotropy of LPCMO films as directly evidenced by LTEM for narrow "zigzag" FM domains[7] coupled to very dense (101)-crystallographic twins for this material in a wide range of temperatures. Such crystal twins, via the wetting effect, promote the occurrence of local "unexpected" CO-FM phases, which we identify in the current work as charge-disordered spin-glass (CD-SG) interfacial states. We also examined transport properties of LPCMO in wide range of temperatures and provide experimental TEM evidence that simple percolation model cannot explain such transport properties at all temperatures below MIT.

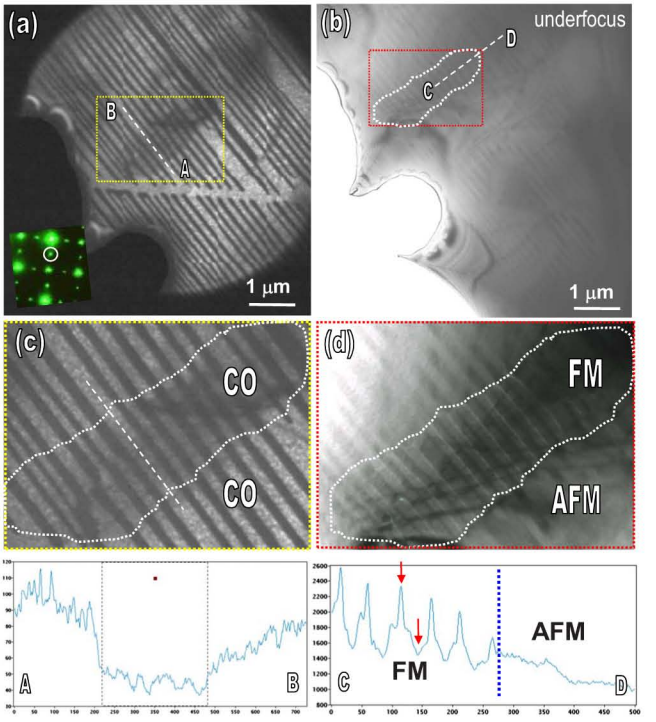

FIG. 1. (Color online) Comparison of the (a) DF and (b) Fresnel images recorded at 160 K showing local mixed CO/FM contrast from the same area of the LPCMO film ($y=0.3$) as outlined by the dashed contours in (a) and (b), and magnified in local images (c) and (d). Here, the area of lower DF(2,0,1/2) contrast outlined by the white-dashed contour in (c) is compared with appropriate FM and AFM contrast observed in the Fresnel image (d). For clarity, the A-B and C-D line scans through the areas of mixed contrast are shown below. The inset in (a) illustrates the diffraction pattern with operating reflections used for DF imaging.

II. EXPERIMENT

Thin LPCMO films of ~200 nm thick were grown on (010)-cut single $NdGaO_3$ (NGO) crystals using the pulsed laser deposition technique described elsewhere.[19] TEM samples were prepared via standard mechanical thinning and polishing techniques to remove the substrate. The final thinning of the films down to perforation hole was performed from the substrate side by using a Fischione ion miller with a single low-voltage argon source at glancing angles and at liquid-nitrogen temperature, which showed amorphous-free surface or very little amorphous component. The structural characterization of samples was undertaken using the JEM2100F-M, a field-emission 200 kV electron microscope with a customized field-free objective lens (residual field <4 Oe). Magnetic and diffraction images were obtained from pure LPCMO films because the NGO substrate was removed by ion milling. For our *in situ* cooling and heating experiment, we used the Gatan cooling stage filled with liquid helium or nitrogen coolant. The LPCMO ($y=0.3$) thin films are orthorhombic (space group *Pnma*) with lattice parameters: $a=5.441$ Å, $b=7.676$ Å, and $c=5.439$ Å. At low temperatures they exhibit a rich variety of physical phenomena, such as phase transitions and electronic-phase separation. On cooling below 220 K, the LPCMO material undergoes a transition from a paramagnetic phase to AFM/CO phase;[3] when the temperature falls below the Curie point ~170 K, a metamagnetic state forms wherein ferromagnetic and antiferromagnetic charge-ordering coexist.

III. TEM OBSERVATIONS NEAR THE MIT

The CO phase in doped manganites above and below MIT ($T_{MI} \sim 164$ K for LPCMO: $y=0.3$) usually is associated with electron charge and orbital order by forming a (2^*a) superstructure below 220 K. Figure 1(a) depicts a typical dark-field (DF) image of the CO phase in an LPCMO film acquired at 160 K using the superlattice (2,0,1/2) reflection of the composite diffraction pattern (DP) shown in the inset. Therefore, in the enlarged DF image of Fig. 1(c) such a CO superstructure appears as crystal lamellae of alternating bright-field and DF contrast along the [101] direction due to the (101) crystal twins. The presence of twin boundaries in LPCMO, in turn, originates from the orthorhombic lattice distortion induced below the structural transition observed at high temperatures.[20] By using DF imaging in $(h/2,0,l/2)$ superlattice reflections [Figs. 1(a) and 1(c)], we can directly

observe the spatial distribution of the CO phase, from which we conclude that this phase is not fully ordered at the nanoscale level [Fig. 1(c)] because of the presence of patched bright contrast within all narrow twin lamellas, typically ~50–150 nm wide. For comparison, in Fig. 1(b) we present a defocused Lorentz image of the same crystal area. A small part of the residual FM domains close to the MIT temperature is magnified in Fig. 1(d).

Of special interest in Figs. 1(c) and 1(d) is a small area outlined by the elliptical white-dashed contour, showing the "unexpected" features of mixed CO/FM contrast in complementary DF [Fig. 1(c)] and Fresnel [Fig. 1(d)] images. The DF-intensity profile along the A-B line in Fig. 1(a) reveals ~50% loss of the average DF intensity when crossing the area inside the contour. On the other hand, the underfocused Fresnel image [Fig. 1(d)], acquired from the same area at defocus value of ~100 μm clearly shows specific magnetic contrast for domain walls (DWs) running exactly along (101)-twin planes in a ~40-nm-thick LPCMO crystal film, where NGO substrate and partly LPCMO film were removed by the low-angular argon ion milling from the substrate side. We note that the line C-D scan across the DWs in Fig. 1(b) reveals the inversion of contrast pattern for FM walls under the changing of defocus sign. Since the whole sample was observed by DF imaging in CO state at this temperature, apparently the ellipticlike region outlined in Figs. 1(c) and 1(d) has visually mixed FM-/CO-phase characteristics, identical to those shown earlier by Loudon *et al.*,[15] who named it as the new CO-FM phase.

To examine the thermal stability of this CO-FM phase, we conducted *in situ* heating and cooling TEM experiments close to MIT, as illustrated in Figs. 2 and 3. First, we heated the sample above the Curie point up to 175 K at the rate of 1 K/min, acquiring DF and Fresnel images at every 4 K interval. Using fixed conditions for Fresnel imaging, we found that the ellipticlike FM state weakened during the heating cycle and its volume fraction shrank with increasing temperature; it finally vanished above 170 K. In contrast, the CO state persisted during heating and grew a little. We noted, at 175 K, the recovery of DF intensity in the ellipticlike CO-FM region, thereby attaining its original contrast with its neighboring areas. Figure 2 details this heating experiment as follows: [Figs. 2(a) and 2(e)] DF images below and above Curie point; [Figs. 2(b)–2(d)] Fresnel images illustrating the melting effect for the FM phase at T=160, 164, and 168 K while approaching the Curie point at ~170 K. We denote the extent of shrinkage of the FM domain cluster by the dashed contour in Figs. 2(b)–2(d). We point out that on cooling this sample back to 160 K [Figs. 3(a) and 3(b)] a partial loss of the DF intensity within ellipticlike areas re-emerges, as outlined by dashed contours in Fig. 3(a). Cooling to 150 K revealed that one such larger area was transformed from a mixed CO-FM state to a pure FM phase while the other small area (the same as that shown in Fig. 2) changed to a pure FM state at temperatures a few degrees lower, thus exhibiting spatial-temperature inhomogeneity in the CO-FM transition process. Upon further cooling, all nucleated FM domains [Fig. 3(b)] continued to grow by consuming more CO-phase areas and merging so that most of the sample was converted into the FM phase. Apparently, the DF and Fresnel

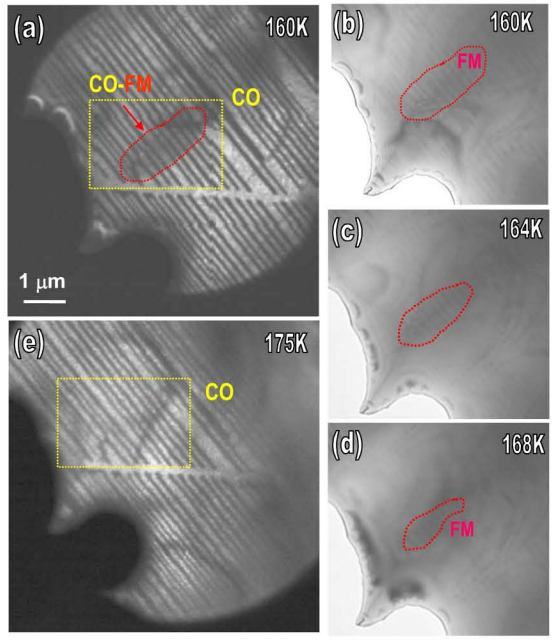

FIG. 2. (Color online) Heating experiment in TEM for LPCMO (010) films illustrating the melting effect for the FM phase close to magnetic Curie point (T_c ~ 170 K). Dark-field images at 160 and 175 K illustrate the change in CO-phase contrast (a) below and (e) above T_c point when the FM domains melt away. In addition, the Fresnel images (b)–(d) recorded from the same LPCMO area show the gradual shrinkage and vanishing of the FM cluster for magnetic domain walls, outlined by the dashed contour, when the magnetic Curie point is reached.

images in Figs. 3(a) and 3(b) are two complementary images for the CO/FM phases involved in the first-order CO-FM transition process. For clarity, we corrected these images for background absorption and aligned them in a single color-composite Fig. 3(c). In Fig. 3(d) we also show two complementary line profiles A-A′ and B-B′ across the (101) crystal twins taken on both sides of the CO-FM phase boundary in Fig. 3(c). We emphasize our very important observation, viz., that the charge and spin-ordering vectors, respectively, lie parallel to the *a* or *c* axis. Furthermore, as exemplified in Fig. 4(d), they appear always to be orthogonal, as is evident from comparing the positions of the bright- and -dark twin CO stripes [Fig. 3(c)] versus the local magnetic moments in FM domains (shown by arrows) following left- and -right zigzag angles for DWs (Ref. 7) in LPCMO.

Already at this point, our *in situ* experiments clearly demonstrate that the so-called CO-FM phase did not exhibit thermodynamic stability or features inherent to individual CO-FM phases, as was claimed in Ref. 15. In fact, as evident in Figs. 1 and 2, upon heating/cooling the sample we observed inhomogeneous nucleation/annihilation and growth of the CO and FM precipitates without formation of the new thermodynamically stable CO-FM phase. However, our intriguing finding is the strong solid-state "wetting" effect within the areas and boundaries of common mixed CO/FM contrast accompanied by partial DF-contrast loss [~50% for outlined area in Fig. 1(c) at 160 K]. Interface wetting and partial melting are known properties of the kinetics

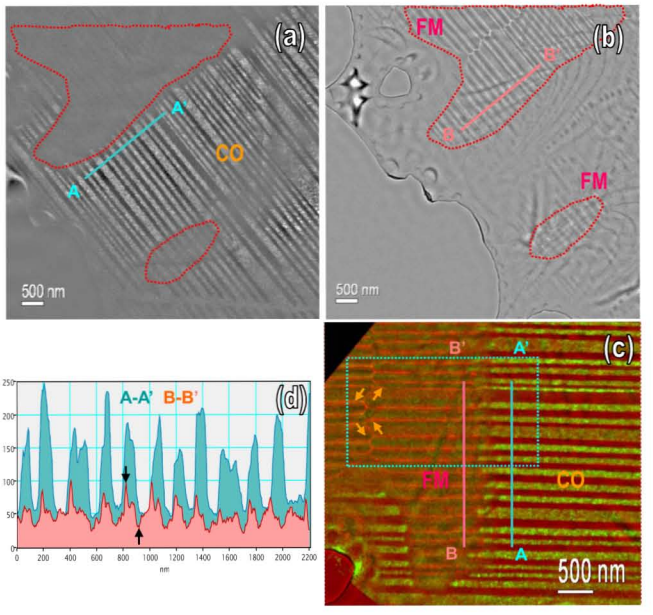

FIG. 3. (Color online) Cooling experiment for LPCMO films: (a) CO phase is observed by DF image recorded with $g(1/2,0,2)$ reflection. (b) Fresnel image from the same area showing two FM domains marked by dashed contours. (c) Composite color image obtained by properly aligning the (a) dark field and (b) Fresnel images showing, respectively, the CO- and FM-phase topography. Notice that all bright domains of the CO phase in (c) are associated with left-tilt zigzag DW in the FM domain while CO dark stripe domains always are associated with right-tilt zigzag DW in FM domain. For clarity, this area is outlined with dotted contour with two parallel A-A′ and B-B′ line scans shown in (d), and presenting the signals for the DF contrast of the CO phase and defocused Fresnel contrast of the FM phase, respectively.

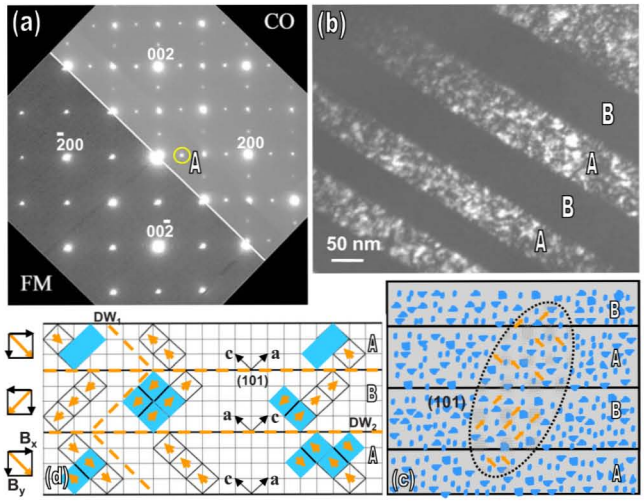

FIG. 4. (Color online) Crystallography and magnetism in LPCMO (010) films. (a) Electron-diffraction patterns of the FM-CO phases naturally coexisting over a wide range of temperatures. (b) Typical high-magnification DF(1/2,0,0) image of the CO phase at $T=160$ K showing inhomogeneous granularlike bright contrast due to incomplete charge order in the CO phase. (c) Morphological model of the FM-phase melting (encircled with elliptical dashed contour), as follows from *in situ* experiments in Figs. 1 and 2, close to the magnetic Curie point. (d) Crystallographic model of the spin-charge ordering in LPCMO for the coexistence of the FM-CO phases, based on our TEM data, including the effects of (101) crystal twins and magnetic domain walls (DW_1/DW_2) formation. Notice that the charge-ordered cells (squares) and spin-ordered cells in the FM domains (arrows) always follow orthogonal directions [for details see Fig. 3(c)].

of phase boundaries accompanying first-order solid-phase transitions.[21,22] In our particular case [Fig. 1(a)], we explain the loss of DF contrast as local "magnetic" melting of the CO phase induced by magnetic moments of nucleated FM precipitates inside CO matrix trying to attain maximal B induction with long-range magnetic order at the expense of partial melting of the soft CO phase through the film thickness. From this viewpoint, it is not surprising that magnetic moments in mixed CO-FM area may carry high spin ordering $\sim 3.5 \pm 0.2$ μ_B/Mn, as measured in Ref. 15 for $La_{0.5}Ca_{0.5}MnO_3$ close to the spin-only value for Mn ions (3.8 μ_B); this correspondence was used to support the idea of the formation of a new CO-FM phase. In our case CO and FM domains may overlap or touch each other as shown by Figs. 1–3 in case of FM domains inside CO matrix. Similar effects in opposite geometry with CO domains inside FM matrix are examined in Fig. 5, which, however, disappear on heating sample (Fig. 6). In both cases, interface wetting is most apparent in overlap geometry, which is also supported by significant statistical observations involved.

IV. SPIN AND CHARGE-ORBITAL ORDERING IN THE TWIN-DOMAIN CONFIGURATION

Figure 4(a) shows the most remarkable electron DPs for coexisting FM and CO phases in LPCMO viewed along the common [010] direction. Formally, the DP herein for the CO phase can be indexed as a supercell $(2a,b,2c)$ with all semi-integer indexes $[h/2,k,l/2]$, $k=0$ belonging to the superstructural reflections. In reality, the DP appears to be a composite emerging from the twin-related switching of unit cells (a,c) and (c,a) for $a \cong c$. As direct evidence for (101) twinning in LPCMO is the typical DF image of the CO phase in superlattice spot A(1/2,0,0) in Fig. 4(b); it clearly distinguishes bright (A-type) and dark (B-type) crystal lamellas divided by (101) twin planes. Here, the bright spots within twin-lamellae A [Fig. 4(b)] show the typical distribution for charge-ordered phase while the complementary dark spots represent CD areas, not contributing to the intensity of DF(1/2,0,0). For the second FM phase examined by LTEM, we also concluded that specific magnetic zigzaglike domain structure[7] is also closely related to presence of (101) crystal twins [see Fig. 3(c)] crated in LPCMO at temperatures below the cubic-to-orthorhombic phase transition at 750–900 °C.[20] Following from our TEM observations, the driving force for strong wetting effect, enhanced by the presence of crystal twins, follows, in fact, from two closely related coexisting and competing ground states: (a) AFM/COI ordering at the scale of few crystal cells [few nanometers in Fig. 4(b)] and (b) FMM ordering, striving to retain a long-range magnetic order within single magnetic domains, for LPCMO ~50–150 nm. This interpretation generates a simple topological model for coexistence of CO-FM phases below Curie

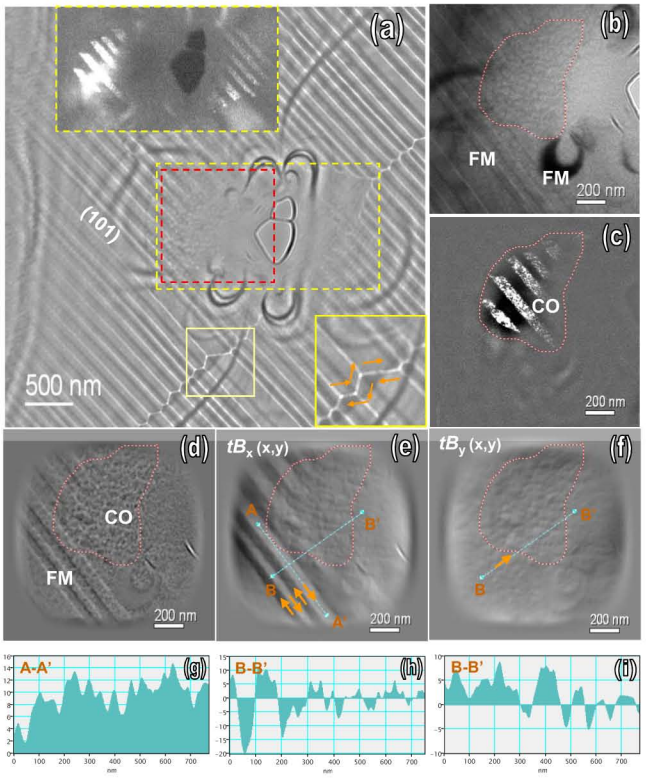

FIG. 5. (Color online) Low-temperature data at $T=11$ K and magnetic-structure analysis of LPCMO by using TIE approach: (a) defocused Fresnel image of the examined area corrected for background, [(b) and (c)] Fresnel and Foucault images of the same area outlined in (a) by a square, (d) differential dI/dz defocused image showing "granular" phase contrast for the CO area, and [(e) and (f)] $[tB_x, tB_y]$ components of the projected magnetic induction $t\boldsymbol{B}(x,y)$ vector map derived from dI/dz image (d) with the appropriate line profiles shown in (g)–(i).

point, as shown in Fig. 4(c). Here, all precipitates of the major CO phase are shown in blue while the minor FM cluster with its specific zigzag spin-domain alignment is outlined by the dashed contour. In contrast, at low temperatures the FM phase particularly is dominant in LPCMO as is apparent from Figs. 5 and 6. Hence, we can propose a crystal model, derived from our TEM data [Fig. 4(d)], showing the principal relationships for spin- and charge-ordering vectors in LPCMO films. Herein, the CO phase precipitates with charge-orbital modulation vector $\vec{q}_{CO}=(2\pi/a)(1/2,0,0)$, in agreement with Figs. 4(a) and 4(b), are depicted by blue $(2a,b,c)$ cells above the square mesh made of primitive perovskite cubic cells. Arrows pointing to the magnetic spin moments for single FM cells (a,b,c) are aligned collinearly to the zigzag Bloch 180° DWs across the (101) twin walls (dashed lines), thus minimizing total magnetostatic energy.[7] We notice that magnetic moments arranged in this way (parallel to local c axis within each twin lamella) always appear to be orthogonal to the charge-orbital ordering vectors (i.e., parallel to the local a axis of the same lamella), based on the TEM data shown in Fig. 3(c). This interpretation is in excellent agreement with the neutron-diffraction solution for the averaged CE-type AFM structure of the CO phase in $La_{0.5}Ca_{0.5}MnO_3$.[23] Our observation is not a trivial one be-

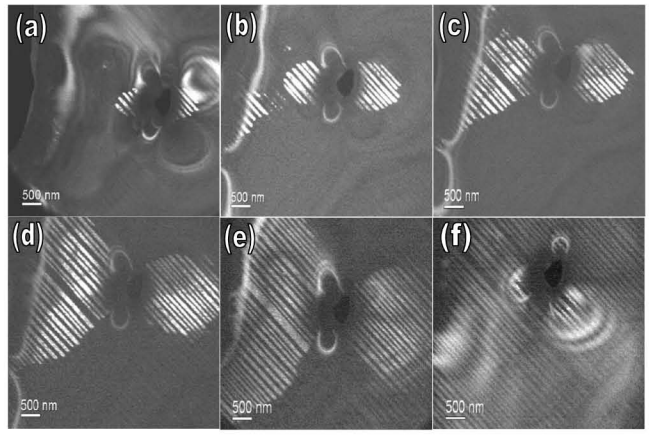

FIG. 6. Dark-field images of the CO phase in LPCMO (010) single-crystal films observed during *in situ* heating TEM experiment. All images taken in $g(2,0,1/2)$ reflection were recorded at the following temperatures: (a) 11 K, (b) 100 K, (c) 115 K, (d) 135 K, (e) 146 K, and (f) 160 K. Notice that in the 11–100 K range, the surface area of the CO phase slowly grows from 3% to 13%. The strongest increase in CO-phase growth begins above 115 K (19%) through 135 K(31%), 146 K (52%), reaching a maximum at ~160 K (97%) at the expense of the FM-phase consumption. The phase boundary for CO-FM phases remains distinguishable, indicating a first-order solid-state phase transition, accompanied by a symmetry change in DPs [for details see also Fig. 3(c)].

cause in another parent compound, $Pr_{0.5}Ca_{0.5}MnO_3$, both vectors of magnetic order and orbital order were defined to be collinear with the a axis,[24] revealing that the La/Pr ratio in $La_{5/8-y}Pr_yCa_{3/8}MnO_3$ manganite (in our case, $y=0.3$ and the ratio $La/Pr>1$) can change both in direction and magnetic order within a single CE-type AFM cell $(2a,b,2c)$ for the orbital ordered $(2a,b,c)$ only CO cell. As we observed, the local microstructure and domain structure in LPCMO are complicated by heavy $(a$-$c)$-crystal twins, which may require further refining of neutron-scattering data[23,24] ignoring these facts, as already predicted in Ref. 23.

In practice, all DF images for the CO-phaselike the one shown in Fig. 4(b) represent a nonuniform granulated contrast, composed of many small bright patches with only a few big bright ones again surrounded with many dark patches. This denotes that the CO phase is strongly inhomogeneous and retains these features down to low temperatures [Fig. 5(c) acquired at $T=11$ K]. On the other hand, the dark patches do not contribute to superlattice DP reflections, and therefore, may behave similarly to the FM phase in Fig. 4(a). This finding indicates that CD states may behave as metamagnetic SG states with essential loss of the magnetic long-range order inherent for the FM phase; we examine this suggestion in more detail below.

In Fig. 5(a) we show a low-temperature Fresnel image for an LPCMO film ($y=0.3$) recorded at 11 K with FM-phase contrast dominating the whole sample over the small remaining CO fraction (~3%), encompassed by a dashed contour in the DF image in the upper inset of this figure. The residual CO-phase domain lies close to the small hole produced by the argon ion milling of sample because only in thin-film area the competing FM phase is unable to establish three-

dimensional full-scale long-range magnetic order. The lower inset in Fig. 5(a) shows the typical zigzag domains for FM phase, greatly reducing magnetostatic energy in absence of stray fields.[7] The central area in Fig. 5(a), outlined by a dashed square and magnified in defocused Fresnel [Fig. 5(b)] and DF [Fig. 5(c)] images, revealed complementary TEM contrasts for the spatially separated FM and CO phases. However, their phase boundary, approximately outlined by the dashed loop, appears weak and uncertain, especially for the FM domains in Fig. 5(b). To examine the FM-CO interfacial properties in LPCMO we took advantage of the "transport-of-intensity" (TIE) approach[25] with a known magnetic solution[26,27] that allows us to recover the object's exit-wave function and, hence, to examine the magnetic properties of the FM-CO interface area described in Figs. 5(d)–5(f). Here Fig. 5(d) shows a pure-phase dI/dz defocused contrast obtained by subtracting carefully aligned under- and over-focused Fresnel images, followed by the magnetic TIE solution presented in Figs. 5(e) and 5(f) by two orthogonal (tB_x, tB_y) components of total projected induction map $tB_i(x,y) \equiv \int B_i(x,y,z)dz (i=x,y)$ expressed in tesla·nanometer units. From the phase-contrast dI/dz image in Fig. 5(d), we clearly see that the "granulated" contrast has spread quite far from the approximate FM-CO phase boundary outlined by the dashed contour. This implies that the long-range magnetic order within FM phase already is degraded in part due to strong mutual wetting at the FM-CO phase boundary, as follows from TIE solution for dI/dz phase contrast in image in Fig. 5(d) presented here by the reconstructed (tB_x, tB_y) maps in images in Figs. 5(e) and 5(f). For clarity, we took two orthogonal scans: Fig. 5(g) A-A′ and Fig. 5(h) B-B′ for $tB_x(x,y)$ map, and one additional scan Fig. 5(i) B-B′ for the $tB_y(x,y)$ map across the CO area. As expected, we observed a positive but oscillating A-A′ x profile in Fig. 5(g) for the positive tB_x components within the FM area along bright-contrast magnetic domains in the reconstructed image Fig. 5(e). The orthogonal B-B′ y scan in Fig. 5(h) shows an alternating change $+tB_x/-tB_x$ of field components across the domain stripes within FM area, which gradually vanish when crossing the CO area. We marked the $+tB_x/-tB_x$ components by orange arrows in Fig. 5(e). Furthermore, the wetting effect modifies the tB_y component in Fig. 5(f), similar to the B-B′ scan across the CO area in Fig. 5(i). Here, tB_y is expected remain positive within the FM area, denoted by the orange arrow outside the dashed contour. However, already it oscillates within FM area and begins to change its sign similar to the B-B′ scan in Fig. 5(e) inside the dashed CO area, suggesting that within the CO-semiconductor area we are observing the magnetic spin-glass (SG) state, and a partial loss of magnetic order in the FM-metallic phase close to the CO-FM interface. In general, the lack of such magnetic order in the SG state produces irregular oscillations of the (tB_x, tB_y) profiles within CO area that, however, become more regular when moving away from CO area and then attain more rectangular-shape profiles expected for FM domains[7] with long-range magnetic order. At present, we conclude that, along with the thermodynamic CO and FM coexisting phases, we also observe metastable CD-SG states proportional to the CO fraction in LPCMO, which display some *intermediate* properties at the smooth interface between the CO and FM phases.

V. TEMPERATURE EVOLUTION OF THE CO PHASE AND ITS RELATION TO MI TRANSITION

Figures 6(a) and 6(f) show a sequence of DF images we recorded with the $g(2,0,1/2)$ superreflection for the CO-phase growth observed in (010) films $La_{5/8-y}Pr_yCa_{3/8}MnO_3$ ($y=0.3$) during the heating from 11 to 160 K. Due to its competition with coexisting FM phase, the growth of CO phase occurs first at thin edges and perforations in the sample. In absence of external fields, the CO phase increases slowly from 3% to 13% between 11–100 K. Its most significant rate of growth begins above ~115 K [Fig. 6(c): 19%] through 135 K [Fig. 6(d): 31%], 146 K [Fig. 6(e): 52%], reaching maximum at ~160 K [Fig. 6(f): 97%]. All this expansion happens at the expense of the FM phase. We measured the evolution of the CO phase, depicted in Figs. 6(a)–6(f), by integrating the CO-phase areas in DF images and plotting them in Fig. 7 (stars). Two independent groups, measuring electrical resistance in crystal films of $La_{5/8-y}Pr_yCa_{3/8}MnO_3$ $(0.27<y<0.4)$, reported similar results.[3,4] We compare our TEM data for the CO fraction in Fig. 7 with the log-resistance curves from Ref. 3. In addition, we made "magnetic" estimates for the amount of the CO [%] phase (not shown in Fig. 7) extracted from magnetic data ($H \leq 1000$ Oe) (Ref. 3) using the approach in Ref. 28. Such estimates are not very accurate in the absence of real magnetic saturation requiring higher magnetic fields.[8,11] Nevertheless, they correctly predicted the growth of the CO phase with temperature in general agreement with direct CO [%] phase TEM measurements in Fig. 6.

Next, we focus only on the reliable TEM data for the CO-phase fraction shown in Fig. 7 (stars). First, we highlight the striking similarity of the CO fraction $f_{CO}(T)$ and the log-resistance $\ln(R/R_{280})$ curve T behavior for LPCMO films with $y=0.3$. Then, assuming similar temperature functions for these curves, $\alpha f_{CO} \propto f(T)$ and $\ln(R/R_{280}) \propto f(T)$, we obtained an empirical relation between the CO fraction and sample resistance $\ln(R/R_{280}) \propto \alpha f_{CO}(T)$ below the MI transition point (~164 K). To the best of our knowledge, this has not been discussed in the literature on LPCMO films. In particular, the strong exponential relation $R(T) = R_{280} \exp[\alpha f_{CO}(T)]$, where α is the scaling constant, already can explain the high-resistance sensitivity to minute changes in the CO fraction, including CD-SG quasistates discussed above. Apparently, small changes in CO phase itself and in the metastable CD-SG states under external magnetic-electrical fields also should induce a strong response in the sample's resistance below the MIT point. Indeed, striking experiments on $1/f$ noise measured by Podzorov *et al.*[9] revealed a many-orders-of-magnitude enhancement of noise for LPCMO ($y=0.3-0.4$) just below the MI transition; the authors explained this by the presence of "percolating phases" that are "FMM and metastable charge-disordered insulations phases." Dhakal *et al.*[4] using electric-resistance data accounted for the MIT transition by the formation of a "fluid phase separated state" at intermediate temperatures. Further, Uehara *et al.*[2] were the first who, for LPCMO pointed to the relations of "percolation phase separation," "colossal magnetoresistance," and "charge-disordered (dark-contrast) nanodomains, … believed to be FM." Finally,

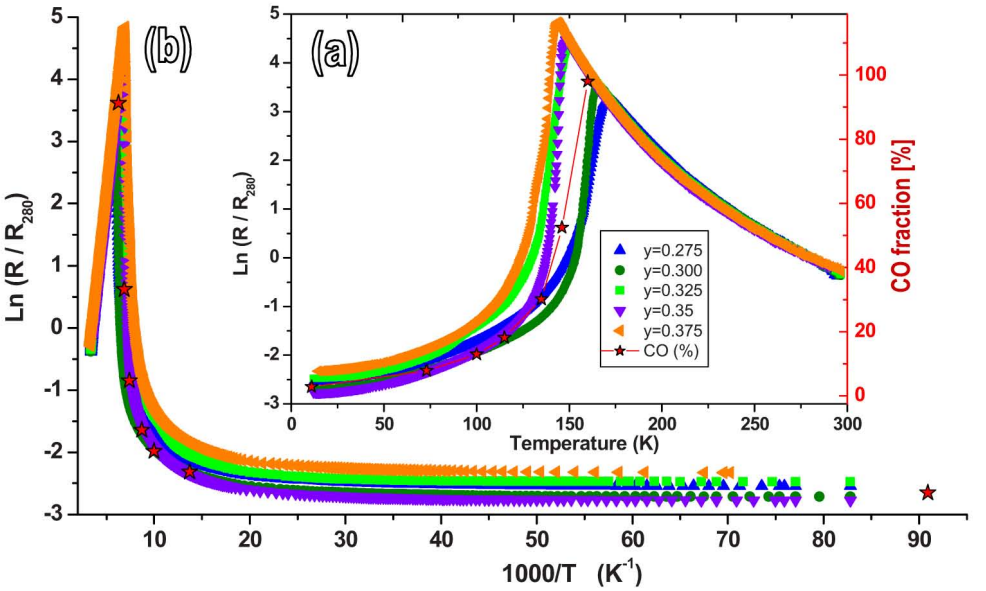

FIG. 7. (Color online) Electrical resistance curves for LPCMO: $0.275 \leq y \leq 0.375$ plotted with color symbols as function of (a) temperature and (b) inverse temperature. They are compared with CO/FM phase balance in LPCMO ($y=0.3$) derived from TEM and shown for the CO-phase fraction by stars. Note the strong empirical correlation, according to which the CO fraction [%] measured by TEM follows closely the log-resistance heating curves for LPCMO ($0.3 \leq y \leq 0.325$) at all temperatures below the MIT peak. Above this peak all resistance curves for the CO phase show semiconductor behavior with a common fixed activation-energy slope (b).

Kiryukhin *et al.*,[17] using synchrotron x-ray diffraction, concluded that "CO phase does not appear to play a major role," however, "…another insulating phase is present," and "MIT is due to the changes … within this latter phase."

VI. INTERPRETATION AND DISCUSSION OF THE EXPERIMENTAL DATA

To better understand our TEM observations and their relationship to transport properties in LPCMO films, including some ideas[2,4,9,17] for possible mechanism of the MI transition, we present the diagram for the MI transition in Fig. 8(a) by using special Arrhenius coordinates (G/G_{280}) versus $(10^3/T)$. We have two special purposes in mind. The first is to show the typical conductance $G(T)$ curve for LPCMO. The second is to analyze the activation energies of competing CO/FM ground states to establish "energy" constraints for conductivity mechanism in LPCMO, since activation barriers appear to be asymptotic lines to $\ln(G/G_{280})$ conductivity plots in special Arrhenius coordinates. Here, for clarity, we plot only single conductance curve from Fig. 7 for crystals $La_{5/8-y}Pr_yCa_{3/8}MnO_3$ ($y=0.3$) using the inverse relation $G(T)=1/R(T)$. For comparison, we also plot, with semired circles, the TEM-derived FM fraction $f_{FM}(T)$, referred to the right-side vertical axis, deduced from the balance $f_{FM}=(1-f_{CO})$ with $f_{CO}(T)$ measured from Fig. 6. Both sets of data were recorded in heating experiments. Again, we observe clear similarity between the log-conductance $\ln(G/G_{280})$ and f_{FM} fraction behavior in the range $160 \rightarrow 11$ K. This also follows from the above empirical relation $G(T)=G_{280}\exp[-\alpha f_{CO}(T)]$, rewritten in another form $\ln(G/G_{280})=\alpha f_{FM}(T)-\alpha$, valid for FM-phase below the MIT point. Both offset constants G_{280} and $-\alpha$ are not essential because we use directly data from Fig. 8(a). Above the MI transition only the CO phase ($T>168$ K) was observed with semiconductorlike decay and activation energy $-E_{CO}=122.1(5)$ meV derived from the $\ln(G/G_{280})$ line slope above MI transition point in Fig. 8(a).

On other hand, well below 73 K the transport is controlled by the metalliclike FM phase with activation energy $E_{FM} \approx 0$ meV, evidenced by horizontal asymptotic limit, defining the maximum saturation for $\ln(G/G_{280})$ curve in the low-T limit ($T \rightarrow 11$ K). Here the region of fast conductivity growth below the MI transition is often cited as "percolation regime." Apparently, the quick growth of conductivity and TEM-observed CO/FM balance changes below MIT should have some relation, which is displayed experimentally, for instance, in Fig. 8(a), by similar temperature curves for $\ln[G(T)/G_{280}]$ and $f_{FM}(T)$ FM fraction in LPCMO at $T<160$ K. For better clarity, we also plot in Fig. 8(b) this relation directly in the parametric form $\ln[G(T)/G_{280}] \approx \alpha f_{FM}(T)$ by using temperature as common parameter in wide range of compositions $0.03<f_{FM}(T)<0.97$ below the MI transition. The experimental points in Fig. 8(b) fit well to the straight line, except one point at $T=146$ K, which deviates from this line by ~2.5 K due to fast changes in sample properties at this temperature. Notice that such coordinates are often used in percolation equations $G \propto (F-F_c)^{s^*}$ for description of percolation transport in metal-insulator mixtures,[29,30] which can be presented in another form suitable for comparison as $\ln G \propto s^* \ln(F-F_c)$, where s^* is the critical exponent and F_c being the critical fraction of conducting phase. Apparently, the log-function $\ln(F-F_c)$ cannot be transformed to linear function f_{FM} used in the observed relation $\ln G \propto f_{FM}$ shown by Fig. 8(b) and valid for all range of $0.03<f_{FM}<0.97$ parameters, no matter what reasonable value of fitting F_c constant should be used. This tells that

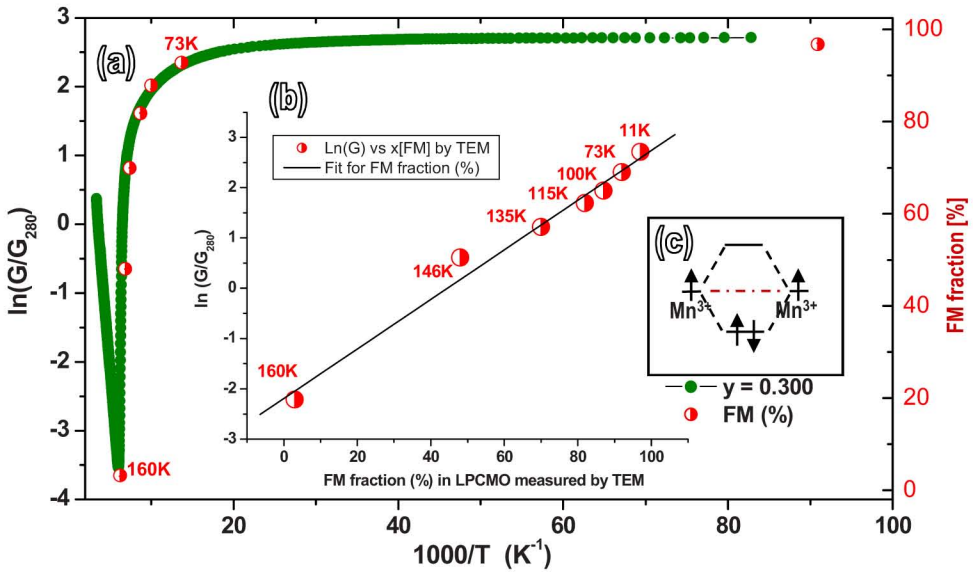

FIG. 8. (Color online) Transport conductivity for MIT in LPCMO. (a) The transport conductance for LPCMO film (y=0.3) is plotted in special Arrhenius coordinates $\ln(G/G_{280})$ vs $10^3/T$ (green circles, referred to left axis) and compared with fraction $f_{FM}[\%]$ of the FM phase (semired circles, referred to the right axis) measured directly by TEM in similar heating experiment. Both sets of experimental data surprisingly follow very similar temperature dependences at all T points below MIT, as shown in better details by appropriate linear relation in the central inset (b). The inset (b) shows experimental relation $\ln[G(T)/G_{280}] \propto \alpha f_{FM}(T)$ for measured conductance and the amount of FM[%] fraction $0.03 < f_{FM}(T) < 0.97$ expressed in parametric form for all common temperatures points used for TEM measurements of the CO/FM fractions in Figs. 5 and 6. (for details see the text). The small inset (c) shows a simplified spin diagram for conducting $e_g(Mn^{3+})$ electrons involved in the spin-exchange (AFM/FM) and orbital- (COI/FMM) ordering effects related to transport properties in LPCMO below the MI transition.

simple percolation approach used for transport description in doped Mott insulators, such as mixed valance manganites, needs further essential revisions.[17] Finally, we do not observe in Fig. 8 any pinning flat steps for $\ln(G)/G_{280}$ curve that would be anticipated if some new "stable" FM-CO phases were present.[15]

The general features of the diagram in Figs. 8(a) and 8(b), reflecting competition between the metal-insulator[18] ground states, also conform the simplest AFM-FM magnetic spin-ordering diagram in Fig. 8(c) for magnetic $Mn^{3+}(t_{2g}^3, e_g^1)$ ions typically involved in cooperative Jahn-Teller (JT) distortions of MnO_6 octahedra, resulting in coexistence of AFM/CO and FM phases in mixed-valence Mn^{3+}/Mn^{4+} manganites. Indeed, Kim and co-workers[31] examined JT distortions in $La_{5/8-y}Pr_yCa_{3/8}MnO_3$ (y=0.375) using Raman optical studies and reported two major types of coexisting distortions. (a) Strong JT distortion ($P2_1/m$ group) associated with AFM/CO phase and (b) weak JT distortion (*Imma* or *Pnma* group) associated with the FM phase. They also found that reversible field-induced magnetic melting transforms the AFM/CO phase into the FM phase at external magnetic fields $B \geq 2$ T. This agrees with our direct observations on local magnetic melting for the AFM/CO phase examined *in situ* by LTEM and DF imaging (Figs. 1, 2, and 5) as mutual wetting and interface melting effects for electronically ordered CO and FM phases coexisting in LPCMO.

Finally, we mention that the complex FM domain structure, observed below the Curie point in LPCMO, as coupled to very dense (101) crystal twins persistent below 750–900 °C,[20] did not receive much attention in most of the original works we cited. However, recently Ward *et al.*[6] reported some interesting transport properties for "…elastically driven anisotropic percolation" in LPCMO (y=0.3) crystal films grown on $NdGaO_3$ substrate, similar to our samples; they showed an extraordinary resistance anisotropy $[(\rho_{[101]} - \rho_{[10\bar{1}]})/\rho_{[10\bar{1}]}] \sim 500\%$ at 110 K with $[10\bar{1}]$ and [101] deduced as the metal and insulator directions. These striking effects were ascribed to "anisotropic strain field;" however, the lattice mismatch for orthorhombic LPCMO(space group *Pnma*), in general, is too small $(a-c)/c = 3.7 \times 10^{-4}$ to explain these observations. More realistically, we should consider the real crystal twins and related FM domain structure of LPCMO. Apparently, the transport of spin-polarized electrons along narrow $[10\bar{1}]$ magnetic domains [Figs. 4(d) and 5(a)] is spin conservative. So, they should behave as metal channels. In contrast, electron-spin transport across crystal twins in the [101] direction is not spin conservative for magnetic domains and, hence, the anisotropy of conductance should be sensitive to additional spin-flipping barriers (ΔE_s) inherent to odd-even FM domains separated by (101) crystal twins, as shown in Figs. 4(d) and 5(a). This should lead in turn to strong resistivity growth along [101] direction measured in Ref. 6. In the limit of high magnetic field[4,8] the AFM/CO phase melts back to the FM state with all magnetic domains washed away, thus leading to strong resistance-anisotropy drop[6] in samples below the MIT.

VII. CONCLUSIONS

We examined the microstructure and magnetic-domain structure in thin epitaxial $La_{5/8-y}Pr_yCa_{3/8}MnO_3$ (y

$=0.275-0.300$) films by Lorentz microscopy methods. Along with the two-phase coexistence in LPCMO films of mesoscopically separated AFM/CO and FM phases in the wide range of temperatures ($11 \leq T \leq 160$ K) below MIT, we also observed some areas of mixed CO-FM contrast, which we interpreted as an interface wetting phenomenon known to exist in first-order phase-transition reactions. Accompanying this effect is the partial magnetic melting of the CO phase at its interface with FM phase, rather than it creating new stable CO-FM phases. Quantitative analyses of the Fresnel images and the TEM data suggest that metastable charge-disordered spin-glass (CD-SG) states form at the wet interfaces of coexisting AFM/CO and FM phases; which should behave as intermediate metastates in specific conductance mechanisms below MIT discussed in the literature for LPCMO films.[2,4,9,16,17] From an energetic viewpoint, these CD-SG metastates do not create new stable CO-FM intermediate phases for MI transition between two ground AFM/CO and FM states, but they can directly contribute to several hysteretic and metastable effects observed for transport properties of LPCMO through the appropriate formation of CD-SG metastates mediating FM domains embedded into CO semiconductor matrix. In particular, from our TEM observations we found that the amount of the CO phase controls the log-resistance curve below the MIT without involving of intermediate stable phases. Such dependence does not follow typical percolation equations, suggesting that percolation model needs further revisions for transport description of manganites. Our results are supported by independent research observations and experimental data reported for LPCMO films.

ACKNOWLEDGMENTS

This work at BNL was supported by the U.S. Department of Energy, Office of Basic Energy Science, under Contract No. DE-AC02-98CH10886. Research in India was supported by grants from the BRNS, Government of India and the Indo-French Centre for Promotion of Advanced Research, New Delhi.

---

*Corresponding authors.
†Present address: Department of Chemistry, Northwestern University, Evanston, Illinois 60208; jiaqing-he@northwestern.edu
‡volkov@bnl.gov
§Present address: Department of Materials Science and Engineering, Nagoya Institute of Technology, Gokisho-cho, Showa-ku, Nagoya 466-8555, Japan.
‖Present address: Nanoscience Center, Department of Physics, University of Jyväskylä, P.O. Box 35, FIN-40014 University of Jyväskylä, Finland.

[1] J. B. Goodenough, Phys. Rev. **100**, 564 (1955).
[2] M. Uehara, S. Mori, C. H. Chen, and S.-W. Cheong, Nature (London) **399**, 560 (1999).
[3] S. Chaudhuri, R. C. Budhani, J. He, and Y. Zhu, Phys. Rev. B **76**, 132402 (2007).
[4] T. Dhakal, J. Tosado, and A. Biswas, Phys. Rev. B **75**, 092404 (2007).
[5] S. Mori, Y. Horibe, T. Asaka, Y. Matsui, C. H. Chen, and S. W. Cheong, J. Magn. Magn. Mater. **310**, 870 (2007).
[6] T. Z. Ward, J. D. Budai, Z. Gai, J. Z. Tischler, L. Yin, and J. Shen, Nat. Phys. **5**, 885 (2009).
[7] J. Q. He, V. V. Volkov, M. Beleggia, T. Asaka, J. Tao, M. A. Schofield, and Y. Zhu, Phys. Rev. B **81**, 094427 (2010).
[8] M. H. Phan, M. B. Morales, N. S. Bingham, H. Srikanth, C. L. Zhang, and S. W. Cheong, Phys. Rev. B **81**, 094413 (2010).
[9] V. Podzorov, M. E. Gershenson, M. Uehara, and S.-W. Cheong, Phys. Rev. B **64**, 115113 (2001).
[10] S.-W. Cheong and H. Y. Hwang, in *Colossal Magnetoresistance Oxides*, Monographs in Condensed Matter Science, edited by Y. Tokura (Gordon and Breach, London, 1999), Chap. 7.
[11] T. Becker, C. Streng, Y. Luo, V. Moshnyaga, B. Damaschke, N. Shannon, and K. Samwer, Phys. Rev. Lett. **89**, 237203 (2002).
[12] S. Mori, R. Shoji, N. Yamamoto, T. Asaka, Y. Matsui, A. Machida, Y. Moritomo, and T. Katsufuji, Phys. Rev. B **67**, 012403 (2003).
[13] J. Tao, D. Niebieskikwiat, M. Varela, W. Luo, M. A. Schofield, Y. Zhu, M. B. Salamon, J. M. Zuo, S. T. Pantelides, and S. J. Pennycook, Phys. Rev. Lett. **103**, 097202 (2009).
[14] C. H. Chen and S.-W. Cheong, Phys. Rev. Lett. **76**, 4042 (1996).
[15] J. C. Loudon, N. D. Mathur, and P. A. Midgley, Nature (London) **420**, 797 (2002).
[16] S. Mori, T. Asaka, and Y. Matsui, J. Electron Microsc. **51**, 225 (2002).
[17] V. Kiryukhin, B. G. Kim, V. Podzorov, S. W. Cheong, T. Y. Koo, J. P. Hill, I. Moon, and Y. H. Jeong, Phys. Rev. B **63**, 024420 (2000).
[18] P. G. Radaelli, R. M. Ibberson, D. N. Argyriou, H. Casalta, K. H. Andersen, S.-W. Cheong, and J. F. Mitchell, Phys. Rev. B **63**, 172419 (2001).
[19] R. C. Budhani, N. K. Pandey, P. Padhan, S. Srivastava, and R. P. S. M. Lobo, Phys. Rev. B **65**, 014429 (2001).
[20] J. Q. He, R. H. Wang, J. N. Gui, and C. Dong, Phys. Status Solidi B **229**, 1145 (2002).
[21] Th. M. Nieuwenhuizen, J. Phys. A **21**, L567 (1988).
[22] R. Lipowsky, Ferroelectrics **73**, 69 (1987); R. Lipowsky and M. E. Fisher, Phys. Rev. B **36**, 2126 (1987).
[23] P. G. Radaelli, D. E. Cox, M. Marezio, and S.-W. Cheong, Phys. Rev. B **55**, 3015 (1997).
[24] Z. Jirak, S. Krupicka, Z. Simsa, M. Dlouha, and S. Vratislav, J. Magn. Magn. Mater. **53**, 153 (1985).
[25] T. E. Gureyev and K. A. Nugent, J. Opt. Soc. Am. A **13**, 1670 (1996); D. Paganin and K. A. Nugent, Phys. Rev. Lett. **80**, 2586 (1998).
[26] V. V. Volkov and Y. Zhu, Phys. Rev. Lett. **91**, 043904 (2003).
[27] V. V. Volkov and Y. Zhu, Ultramicroscopy **98**, 271 (2004).
[28] N. Kallel, N. Ihzaz, S. Kallel, A. Hagaza, and M. Oumezzine, J. Magn. Magn. Mater. **321**, 2285 (2009).
[29] D. S. McLachlan, J. Phys. C **20**, 865 (1987); V. Hardy, A. Wahl, and C. Martin, Phys. Rev. B **64**, 064402 (2001).
[30] S. Kirkpatrick, Rev. Mod. Phys. **45**, 574 (1973); I. Webman, J. Jortner, and M. H. Cohen, Phys. Rev. B **14**, 4737 (1976).
[31] M. Kim, H. Barath, S. L. Cooper, P. Abbamonte, E. Fradkin, M. Rübhausen, C. L. Zhang, and S.-W. Cheong, Phys. Rev. B **77**, 134411 (2008).